Bloch oscillations and nonlinear transport in a one-dimensional semiconductor superlattice

S. K. Lyo*
Sandia National Laboratories, Albuquerque, New Mexico 87185, USA
(Received 22 January 2008; revised manuscript received 20 March 2008; published 8 May 2008)

We present an exact analytic result for the time-dependent and steady-state current and the distribution function in a nonlinear electric field for an electron gas in a one-dimensional superlattice miniband by employing a relaxation-time approximation for inelastic scattering. Our transparent results clearly show the condition for the onset of the Bloch oscillations, the field for the peak steady-state current, and the distinct roles played by elastic and inelastic scattering for the damped oscillations and the steady-state current. The results are consistent with a recent full microscopic numerical calculation.

DOI: 10.1103/PhysRevB.77.195306 PACS number(s): 72.20.Ht, 73.63.Nm, 72.10.Bg

I. INTRODUCTION

Electrons driven by a high electric field E sweep through a Bloch band and yield oscillations in k space as well as in real space. The oscillations are damped before the electrons sweep through the band many times because of scattering, reaching a steady state and yielding the negative differential conductance. This fascinating phenomenon has received much attention in the past for its potential to yield terahertz generation and also for applications to negative differential conductance.[1–14] Esaki and Tsu[1] predicted that negative differential conductance can be observed in semiconductor superlattices without applying a huge electric field due to their large lattice periods, small Brillouin zones, and narrow bandwidths. Investigations of Bloch oscillations were carried out in terahertz emission,[15–18] electro-optic detection,[18,19] and a four-wave mixing experiment.[20]

In an extremely high field wherein the potential energy drop between the superlattice cells is larger than the bandwidth, a full quantum mechanical approach in terms of Wannier–Stark ladders is convenient and conduction occurs through phonon-assisted hopping down the Stark ladder.[12,21] In the opposite (but still nonlinear) limit, however, a semiclassical formalism based on the Boltzmann equation is preferable in studying the scattering effect. It is difficult to consider the interband tunneling effect in this approach. This effect is negligible if the band gap is very large. In this paper, we present an exact analytic result for the time-dependent current and the distribution function in the latter nonlinear limit for a degenerate and nondegenerate electron gas in a one-dimensional superlattice miniband by employing a relaxation-time approximation for inelastic scattering with a constant (i.e., energy independent) relaxation rate. The current model is relevant to a quantum wire with a periodically modulated potential. The final transparent analytic results clearly show the distinct roles played by elastic and inelastic scattering in competition with the driving force for the damped Bloch oscillations and the steady-state current. They also quantitatively show how scattering damps the Bloch oscillation, the condition for the onset of the oscillations, and the oscillation frequency. The present approach can serve as a guide in understanding the results of a more complicated full numerical treatment. A recent full numerical study that replaces the present relaxation-time approximation of inelastic scattering by microscopic electron-phonon scattering processes yielded results very similar to those predicted here.[22] A similar relaxation-time approach based on an iterative numerical solution[10] was employed earlier for a three-dimensional system for the steady-state current and yielded results qualitatively similar to those based on a microscopic treatment.[8]

The organization of the paper is as follows: The basic model is introduced in Sec. II, wherein a general formalism for the steady-state current is presented. The time-dependent current as well as the steady-state current is obtained in Sec. III, while the time-dependent distribution function is given in Sect IV. The numerical studies of the results and discussions are presented in Sec. V. Finally, a brief summary is given in Sec. VI.

II. RELAXATION-TIME MODEL

While our model can be generalized to multibands, we will study only the single-band situation for clarity. The time-dependent rate equation for the distribution function $f(k,t)$ is given by

$$\frac{\partial f(k,t)}{\partial t} - \frac{eE}{\hbar}\frac{\partial f(k,t)}{\partial k} = -\nu_{\text{in}}[f(k,t) - f^{(0)}(\varepsilon_k)] - \nu_{\text{el}}(k)[f(k,t) - f(-k,t)], \quad (1)$$

where ν_{in} is a phenomenological inelastic scattering rate assumed to be a constant,[10] $f^{(0)}(\varepsilon_k)$ is the Fermi function, and $\nu_{\text{el}}(k)$ is the elastic scattering rate given by

$$\nu_{\text{el}}(k) \equiv \frac{\pi}{2\hbar}|U(2k)|^2 D(\varepsilon_k). \quad (2)$$

Here, $U(2k)$ and $D(\varepsilon_k)$ are the matrix elements for the backscattering and the density of states at an energy ε_k, respectively. The total particle number is conserved in Eq. (1) at all times. In this paper, we obtain the steady-state current for an arbitrary scattering potential $U(2k)$ and the time-dependent current as well as the distribution function for a constant ν_{el}. In the present one-dimensional lattice, the expression for elastic scattering in Eq. (1) is exact, in contrast to the past studies in three dimensions. In the latter case, a similar backscattering model $\nu_{\text{el}}[f(\mathbf{k},t) - f(-\mathbf{k},t)]$ was employed by Kti-

torov *el al.*[2] for a constant $\nu_{\rm el}$, neglecting elastic scattering to other directions. Similarly, Ignatov *et al.*[9] studied the elastic momentum-relaxation model $\nu_{\rm el}[f(k_z,t)-f(-k_z,t)]$, where $\hbar k_z$ is the crystal momentum in the direction of the electric field.

Defining

$$F^{\pm}(x,t)=[f(k,t)\pm f(-k,t)]/2, \tag{3}$$

from Eq. (1) we obtain

$$\frac{\partial F^{+}(x,t)}{\partial t}-\frac{\partial F^{-}(x,t)}{\partial x}=-\nu_{\rm in}[F^{+}(x,t)-f^{(0)}(\varepsilon_k)], \tag{4}$$

and

$$\frac{\partial F^{-}(x,t)}{\partial t}-\omega_E\frac{\partial F^{+}(x,t)}{\partial x}=-\tilde{\nu}(k)F^{-}(x,t), \tag{5}$$

where $\omega_E=eEa/\hbar$, $x=ka$, a is the superlattice period, and

$$\tilde{\nu}(k)=\nu_{\rm in}+2\nu_{\rm el}(k). \tag{6}$$

We now carry out the Laplace transformation for the above expressions by employing the notation

$$\mathcal{F}^{\pm}(x,s)=\int_0^{\infty}F^{\pm}(x,t)e^{-{\rm st}}dt. \tag{7}$$

By using the initial conditions $F^{-}(x,0)=0$, $F^{+}(x,0)=f^{(0)}(\varepsilon_k)$, we find

$$\omega_E\frac{\partial\mathcal{F}^{-}(x,s)}{\partial x}=(\nu_{\rm in}+s)\mathcal{F}^{+}(x,s)-\left(1+\frac{\nu_{\rm in}}{s}\right)f^{(0)}(\varepsilon_k), \tag{8}$$

and

$$\omega_E\frac{\partial\mathcal{F}^{+}(x,s)}{\partial x}=[\tilde{\nu}(k)+s]\mathcal{F}^{-}(x,s). \tag{9}$$

From Eqs. (8) and (9), we then find

$$\frac{\partial^2\mathcal{F}^{-}(x,s)}{\partial x^2}=A(x)\mathcal{F}^{-}(x,s)-C\frac{\partial f^{(0)}[\varepsilon(x)]}{\partial x}, \tag{10}$$

where

$$A(x)=(\nu_{\rm in}+s)[\tilde{\nu}(k)+s]/\omega_E^2,\quad C=\left(1+\frac{\nu_{\rm in}}{s}\right)/\omega_E. \tag{11}$$

Equation (10) is solved by expanding

$$\mathcal{F}^{-}(x,s)=\sum_{m=1}^{\infty}\mathcal{F}_m^{-}(s)\sin(mx),$$

$$\mathcal{F}_m^{-}(s)=\frac{2}{\pi}\int_0^{\pi}\mathcal{F}^{-}(x,s)\sin(mx)dx, \tag{12}$$

$$A(x)=\sum_{m=0}^{\infty}A_m\cos(mx),$$

$$A_m=\frac{2}{\pi(1+\delta_{m,0})}\int_0^{\pi}A(x)\cos(mx)dx, \tag{13}$$

and

$$f^{(0)}[\varepsilon(x)]=\sum_{m=0}^{\infty}f_m^{(0)}\cos(mx),$$

$$f_m^{(0)}=\frac{2}{\pi(1+\delta_{m,0})}\int_0^{\pi}f^{(0)}[\varepsilon(x)]\cos(mx)dx. \tag{14}$$

By inserting Eqs. (12)-(14) in Eq. (10), we find

$$\hat{\mathcal{F}}^{-}(s)=-C\hat{B}(s)^{-1}\hat{f}^{(0)}, \tag{15}$$

where $\hat{\mathcal{F}}^{-}(s)=\mathrm{col}(\mathcal{F}_1^{-}(s),\mathcal{F}_2^{-}(s),\mathcal{F}_3^{-}(s),\ldots)$, $\hat{f}^{(0)}=\mathrm{col}(f_1^{(0)},2f_2^{(0)},3f_3^{(0)},\ldots)$ are column vectors and $\hat{B}(s)$ is a symmetric square matrix given by

$$\hat{B}(s)_{n,m}=(n^2+A_0)\delta_{n,m}+\frac{1}{2}[-A_{n+m}+A_{|n-m|}(1-\delta_{n,m})],$$

$$m,n=1,2,3,\ldots. \tag{16}$$

If $\nu_{\rm el}(k)=\nu_{\rm el}$ is independent of k, Eq. (16) simply reduces to $\hat{B}(s)_{n,m}=(n^2+A_0)\delta_{n,m}$, yielding

$$\mathcal{F}_n^{-}(s)=-C\frac{nf_n^{(0)}}{n^2+A_0},\quad A_0=(\nu_{\rm in}+s)(\nu_{\rm in}+2\nu_{\rm el}+s)/\omega_E^2. \tag{17}$$

For a tight-binding band structure, we consider

$$\varepsilon(x)=-\sum_{n=0}^{\infty}t_n\cos nx. \tag{18}$$

The time-dependent current is given by

$$J(t)=-\frac{e}{\pi}\int_{-\pi}^{\pi}\partial\varepsilon(x)/(\hbar\,\partial x)f(k,t)dx$$

$$=-\frac{e}{\hbar\pi}\sum_{n=1}^{\infty}nt_n\int_{-\pi}^{\pi}\sin nxf(k,t)dx.$$

By changing the sign $x\to -x$ for the interval $(-\pi,0)$ and by using Eq. (3), we find

$$J(t)=-\frac{e}{\hbar}\sum_{n=1}^{\infty}nt_nF_n^{-}(t),\quad F_n^{-}(t)=\frac{2}{\pi}\int_0^{\pi}\sin nxF^{-}(x,t)dx. \tag{19}$$

For later numerical applications, we will adopt a single mode approximation and consider only the fundamental mode $n=1$ for simplicity,

$$\varepsilon(x) = \frac{\Delta}{2}(1 - \cos x), \tag{20}$$

where $t_0 = -t_1 = -\Delta/2$ in Eq. (18). The Laplace transform of $J(t)$ is given by

$$\mathcal{J}(s) = -\frac{e}{\hbar}\sum_{n=1}^{\infty} n t_n \mathcal{F}_n^-(s). \tag{21}$$

The steady-state current equals

$$J(t=\infty) = \lim_{s\to 0} s\mathcal{J}(s) = -\frac{e}{\hbar}\sum_n n t_n \lim_{s\to 0} s\mathcal{F}_n^-(s), \tag{22}$$

which can be found from Eq. (15),

$$\lim_{s\to 0} s\hat{\mathcal{F}}^-(s) = -\frac{\nu_{\rm in}}{\omega_E}\hat{B}(0)^{-1}\hat{f}^{(0)}. \tag{23}$$

For the simple case wherein $\nu_{\rm el}(k) = \nu_{\rm el}$ is independent of k, Eq. (22) reduces in view of Eq. (17) to

$$J(t=\infty) = \frac{e}{\hbar}\sum_{n=1}^{\infty} n^2 t_n \frac{\nu_{\rm in}\omega_E f_n^{(0)}}{n^2\omega_E^2 + \nu_{\rm in}\nu_{\rm tr}}, \tag{24}$$

where $\nu_{\rm tr} = \nu_{\rm in} + 2\nu_{\rm el}$ is the total transport relaxation rate.

III. TIME-DEPENDENT CURRENT

In this section, we study the time-dependent current for the special case wherein the scattering rates are independent of k. In this case, we find from Eqs. (17) and (21),

$$\mathcal{J}(s) = \frac{e}{\hbar}\left(1 + \frac{\nu_{\rm in}}{s}\right)\sum_{n=1}^{\infty} \frac{n^2 t_n \omega_E f_n^{(0)}}{n^2\omega_E^2 - \nu_{\rm el}^2 + (s+\nu_t)^2}, \tag{25}$$

where $\nu_t = \nu_{\rm in} + \nu_{\rm el}$ is the total scattering rate. We find a damped nonoscillatory current for the low-field regime $\nu_{nE<}^2 \geq 0$ and a damped oscillatory solution for the high-field regime $\nu_{nE>}^2 > 0$ defined by

$$\nu_{nE<} = \sqrt{\nu_{\rm el}^2 - n^2\omega_E^2}, \quad n\omega_E \leq \nu_{\rm el},$$
$$\nu_{nE>} = \sqrt{n^2\omega_E^2 - \nu_{\rm el}^2}, \quad n\omega_E > \nu_{\rm el}. \tag{26}$$

The inverse Laplace transform of Eq. (25) yields

$$J(t) = \frac{e\omega_E}{\hbar}\sum_{n=1}^{\infty} n^2 t_n f_n^{(0)} \times\left[\frac{\nu_{\rm in}}{n^2\omega_E^2 + \nu_{\rm in}\nu_{\rm tr}} + \exp(-\nu_t t)\left(\frac{\sinh(\nu_{nE<}t)}{\nu_{nE<}} - \frac{\nu_{\rm in}}{\nu_{nE<}}\frac{\nu_t \sinh(\nu_{nE<}t) + \nu_{nE<}\cosh(\nu_{nE<}t)}{n^2\omega_E^2 + \nu_{\rm in}\nu_{\rm tr}}\right)\right], \quad n\omega_E \leq \nu_{\rm el}. \tag{27}$$

By replacing $\nu_{nE<} \to i\nu_{nE>}$ in the above expression, we find

$$J(t) = \frac{e\omega_E}{\hbar}\sum_{n=1}^{\infty} n^2 t_n f_n^{(0)}\left[\frac{\nu_{\rm in}}{n^2\omega_E^2 + \nu_{\rm in}\nu_{\rm tr}} + \exp(-\nu_t t)\times\left(\frac{\sin(\nu_{nE>}t)}{\nu_{nE>}} - \frac{\nu_{\rm in}}{\nu_{nE>}}\frac{\nu_t \sin(\nu_{nE>}t) + \nu_{nE>}\cos(\nu_{nE>}t)}{n^2\omega_E^2 + \nu_{\rm in}\nu_{\rm tr}}\right)\right], \quad n\omega_E > \nu_{\rm el}. \tag{28}$$

The oscillatory contribution to the current in Eq. (28) appears starting from high values of n for a given electric field. The steady-state solution represented by the first terms in Eqs. (27) and (28) is identical to the expression in Eq. (24). Damped Bloch oscillations and the steady-state current were also studied by previous authors in three dimensions.[2,9,12–14]

In the remaining part of this section, we study some interesting properties of the time-dependent solution and the steady-state current by employing the single mode approximation $n=1$. It is interesting to note that the oscillation of the current is possible only in the high-field limit $\omega_E > \nu_{\rm el}$ when the Bloch frequency exceeds the elastic scattering rate. The condition for the onset of the oscillation depends only on the elastic scattering rate that tries to prevent the electrons from completing the cyclic motion in the Brillouin zone by reversing the direction of the motion. Visible oscillations of the current can be seen only at high fields when the oscillation rate $\nu_{1E>}$ is much larger than the damping rate ν_t. In the limit $E \to 0$, the current reduces to the linear response result $J \propto \tau_{\rm tr}$. For high fields $\omega_E \gg \sqrt{\nu_{\rm in}\nu_{\rm tr}}$, Eq. (24) reduces to

$$J(t=\infty) = \frac{e\nu_{\rm in}\Delta}{2\hbar\omega_E} f_1^{(0)}. \tag{29}$$

Namely, the steady-state current becomes linear in $\nu_{\rm in}$ and is independent of the elastic scattering rate. It can be shown that, in general, the high-field current is linear in the strength of the inelastic scattering rate, independent of elastic scattering, and inversely proportional to the field beyond the relaxation-time approximation. The proof directly follows from Eq. (1) as well from a microscopic expression for the electron-phonon scattering rate for the first term therein. In the high-field limit and for the steady state at $t=\infty$, we note that the gradient of the distribution function $\partial f(k,t)/\partial k$ in Eq. (1) is very small, yielding a nearly uniform distribution $f(k,t) = f_\infty + \mathcal{O}(1/\omega_E)$, where $f_\infty = f_0^{(0)}$ is a constant defined in Eq. (14). Equation (1) can then be approximated to the first order in $1/\omega_E$ as

$$\frac{\partial f(k,t)}{\partial x} \simeq -\frac{\nu_{\rm in}}{\omega_E}[f^{(0)}(\varepsilon_k) - f_0^{(0)}],$$

yielding Eq. (29) via Eqs. (14) and (19). The basic argument for the absence of the effect of the elastic scattering on the high-field current in general relies on the fact that the initial equilibrium function $f_k^{(0)}$ as well as the steady-state distribution function $\simeq f_\infty$ cancels out from the elastic scattering term of the Boltzmann equation due to energy conservation.

The steady-state current in Eq. (24) becomes maximum at

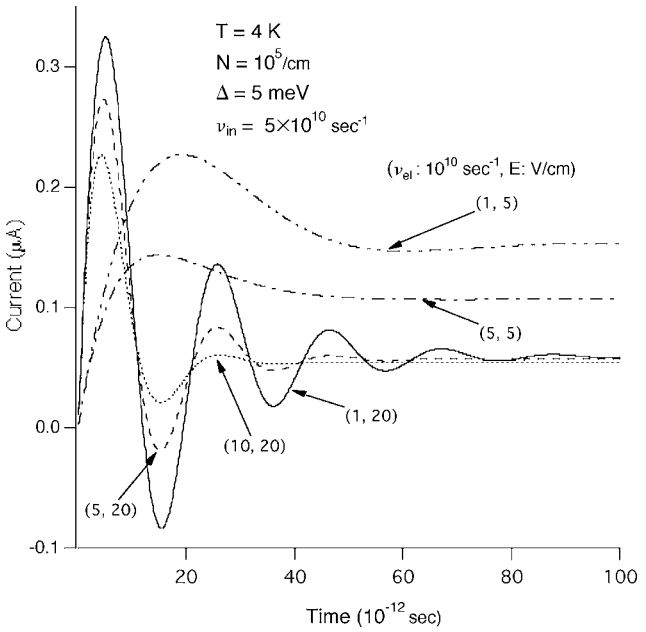

FIG. 1. The current as a function of the time for the inelastic scattering rate $\nu_{\rm in}=5\times10^{10}$ s^{-1} and the bandwidth $\Delta=5$ meV for several values of $(\nu_{\rm el},E)$, where $\nu_{\rm el}$ is the elastic scattering rate in 10^{10} s^{-1} and E is the electric field in V/cm.

$$\omega_E=\sqrt{\nu_{\rm in}/\tau_{\rm tr}} \tag{30}$$

and equals

$$J_{\rm max}=\frac{e\Delta}{4\hbar}f_1^{(0)}\sqrt{\nu_{\rm in}\tau_{\rm tr}}. \tag{31}$$

The optimum current condition in Eq. (30) requires that the Bloch frequency equal $1/2\pi$ times the geometric average of the inelastic scattering rate and the transport relaxation rate. The maximum current becomes independent of the inelastic scattering rate for $\nu_{\rm in}\gg\nu_{\rm el}$ but decreases as $\sqrt{\nu_{\rm in}/\nu_{\rm el}}$ in the opposite limit. Equations (30) and (31) satisfy the correct scaling properties of Eq. (1); multiplying the inelastic and elastic scattering rates in Eq. (1) by a constant has the effect of multiplying the field on the left hand side therein and that of Eq. (30) by the same constant, while there is no other effect for the steady-state current as in Eq. (31). A recent full numerical study that microscopically treated the first (inelastic scattering) term of Eq. (1) in terms of electron-phonon scattering yielded results numerically similar to those given by Eqs. (24) and (29)–(31) in their scale dependences on the inelastic and elastic scattering rates and ω_E.[22]

IV. TIME-DEPENDENT DISTRIBUTION FUNCTION

The time-dependent distribution function is given by

$$f(k,t)=\sum_{n=0}^{\infty}[F_n^-(t)\sin(nx)+F_n^+(t)\cos(nx)], \tag{32}$$

where $F_n^-(t)$ was defined earlier and $F_n^+(t)$ is the expansion coefficients for

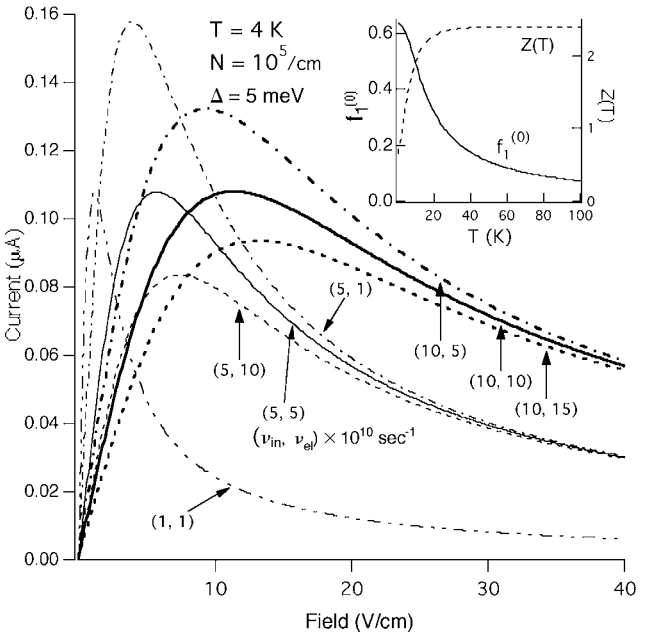

FIG. 2. The steady-state current as a function of the field for several values of energy-independent scattering rates $(\nu_{\rm in},\nu_{\rm el})$ in units of 10^{10} s^{-1} and the bandwidth $\Delta=5$ meV. The upper right inset shows the temperature dependences of $f_1^{(0)}$ (left axis) and the current $J\propto Z(T)$ (right axis) at high fields in the negative–differential-conductance region. The quantity $Z(T)$ is defined in the text.

$$F^+(x,t)=\sum_{n=0}^{\infty}F_n^+(t)\cos(nx),$$
$$F_n^+(t)=\frac{2}{\pi(1+\delta_{n,0})}\int_0^{\pi}F^+(x,t)\cos(nx)dx. \tag{33}$$

From Eqs. (7), (8), (17), and (33), we find

$$\mathcal{F}_n^+(s)=-\frac{1}{s}\frac{n^2\omega_E^2f_n^{(0)}}{n^2\omega_E^2+(\nu_{\rm in}+s)(\nu_{\rm in}+2\nu_{\rm el}+s)}+\frac{1}{s}f_n^{(0)}, \tag{34}$$

and

$$\mathcal{F}_n^-(s)=-\left(1+\frac{\nu_{\rm in}}{s}\right)\frac{n\omega_Ef_n^{(0)}}{n^2\omega_E^2+(\nu_{\rm in}+s)(\nu_{\rm in}+2\nu_{\rm el}+s)}. \tag{35}$$

The inverse Laplace transform of Eqs. (34) and (35) proceeds as before, yielding for the low-field case,

$$F_n^+(t)=-\frac{n^2\omega_E^2f_n^{(0)}}{n^2\omega_E^2+\nu_{\rm in}\nu_{\rm tr}}\left(1-\exp(-\nu_t t)\frac{1}{\nu_{nE<}}[\nu_t\sinh(\nu_{nE<}t)+\nu_{nE<}\cosh(\nu_{nE<}t)]\right)+f_n^{(0)},$$
$$n\omega_E\le\nu_{\rm el}, \tag{36}$$

and for the high-field case,

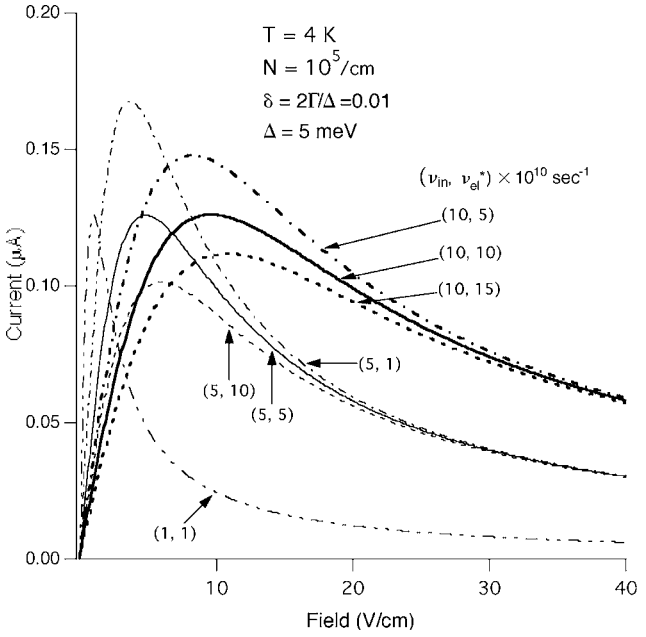

FIG. 3. The steady-state current as a function of the field for the case wherein the elastic scattering matrix element is independent of the momentum transfer for several values of the scattering rates $(\nu_{\rm in}, \nu_{\rm el}^*)$ in units of 10^{10} s^{-1}. Here, $\nu_{\rm el}^*$ is the elastic scattering rate at the band center, Δ is the bandwidth, and Γ is the level damping introduced to avoid the one-dimensional van Hove singularity in the density of states.

$$F_n^+(t) = -\frac{n^2\omega_E^2 f_n^{(0)}}{n^2\omega_E^2 + \nu_{\rm in}\nu_{\rm tr}}\left(1 - \exp(-\nu_t t)\frac{1}{\nu_{nE>}}[\nu_t \sin(\nu_{nE>}t) + \nu_{nE>}\cos(\nu_{nE>}t)]\right) + f_n^{(0)},$$

$$n\omega_E > \nu_{\rm el}. \tag{37}$$

For the low-field case, we also find

$$F_n^-(t) = -n\omega_E f_n^{(0)}\left[\frac{\nu_{\rm in}}{n^2\omega_E^2 + \nu_{\rm in}\nu_{\rm tr}} + \exp(-\nu_t t)\left(\frac{\sinh(\nu_{nE<}t)}{\nu_{nE<}} - \frac{\nu_{\rm in}}{\nu_{nE<}}\frac{\nu_t \sinh(\nu_{nE<}t) + \nu_{nE<}\cosh(\nu_{nE<}t)}{n^2\omega_E^2 + \nu_{\rm in}\nu_{\rm tr}}\right)\right],$$

$$n\omega_E \le \nu_{\rm el} \tag{38}$$

and for the high-field case,

$$F_n^-(t) = -n\omega_E f_n^{(0)}\left[\frac{\nu_{\rm in}}{\nu_t^2 + n^2\omega_E^2 - \nu_{\rm el}^2} + \exp(-\nu_t t)\left(\frac{\sin(\nu_{nE>}t)}{\nu_{nE>}} - \frac{\nu_{\rm in}}{\nu_{nE>}}\frac{\nu_t \sin(\nu_{nE>}t) + \nu_{nE>}\cos(\nu_{nE>}t)}{n^2\omega_E^2 + \nu_{\rm in}\nu_{\rm tr}}\right)\right],$$

$$n\omega_E > \nu_{\rm el}. \tag{39}$$

Note that the last term $\propto f_n^{(0)}$ in Eqs. (36) and (37) inserted in Eq. (32) yields the equilibrium Fermi function $f^{(0)}(\varepsilon_k)$.

The quantity $f_n^{(0)}$ can be evaluated for a general monotonous band at low temperatures $T \ll \varepsilon_b$, where ε_b is the bandwidth, yielding

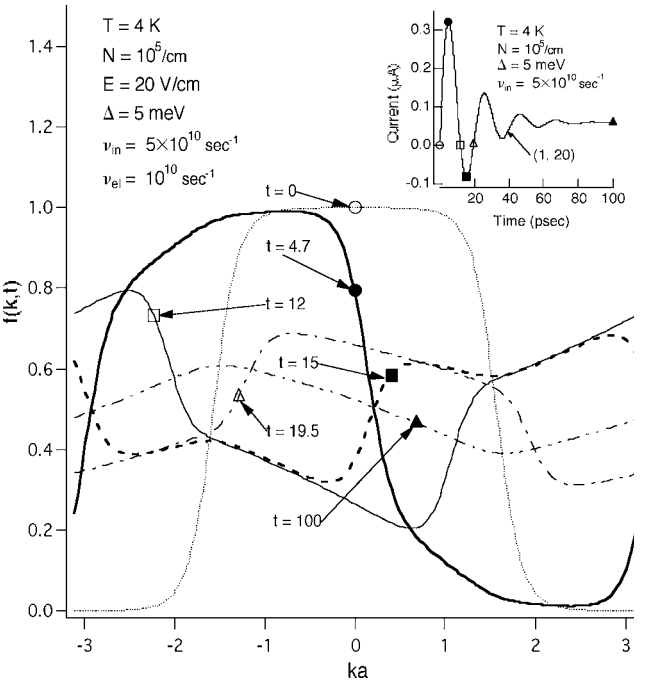

FIG. 4. The evolution of the distribution function $f(k,t)$ at several time points (represented by the symbols, each lying on the concomitant curve) in units of picosecond for the electric field $E=20$ V/cm, the bandwidth $\Delta=5$ meV, and the energy-independent scattering rates $\nu_{\rm in}=5\times10^{10}$ s^{-1} and $\nu_{\rm el}=10^{10}$ s^{-1}, relevant for the solid curve in Fig. 1. The symbols in the inset show the current from Fig. 1 at these time points for $(\nu_{\rm el},E)=(1,20)$ where $\nu_{\rm el}$ is in 10^{10} s^{-1} and E is in V/cm.

$$f_n^{(0)} = \frac{2a_n \sin(nx_\mu)}{n(1+\delta_{n,0})\sinh(\pi a_n)}, \tag{40}$$

where $a_n = nk_BT/\varepsilon'(x_\mu)$, $\varepsilon'(x) = d\varepsilon(x)/dx$, $\varepsilon(x_\mu) \equiv \mu$, and μ is the chemical potential. The current model yields $\varepsilon'(x_\mu) = \Delta \sin(x_\mu)/2$.

V. NUMERICAL STUDIES AND DISCUSSIONS

For numerical studies, we consider the energy dispersion in Eq. (20) for simplicity and assume $a=100$ nm. The quantities $f_m^{(0)}$ in Eq. (14) are evaluated numerically. We first present numerical results for the case wherein $\nu_{\rm el}$ is a constant. The time-dependent current given in Eqs. (27) and (28) is displayed in Fig. 1 for $\nu_{\rm in}=5\times10^{10}$ s^{-1} for several values of $(\nu_{\rm el},E)$, wherein $\nu_{\rm el}$ is in units of 10^{10} s^{-1} and the electric field is in V/cm. A large total scattering rate ν_t quickly damps the current oscillation. Therefore, pronounced oscillations are seen only for small $\nu_{\rm el}$ and large E, such as, for example, for $(\nu_{\rm el},E)=(1,20)$ (solid curve). The role of the lattice period in our model is to set the scale of E through the quantity Ea, which satisfies $Ea \ll \Delta$. For the upper two dashed-dotted and dashed–double-dotted curves, the oscillation is not visible because the oscillation frequency $\nu_{1E>}$ [defined in Eq. (26)] is too small. The asymptotic currents for the lower three curves corresponding to the high field $E=20$ V/cm are similar in magnitude and become nearly independent of $\nu_{\rm el}$,

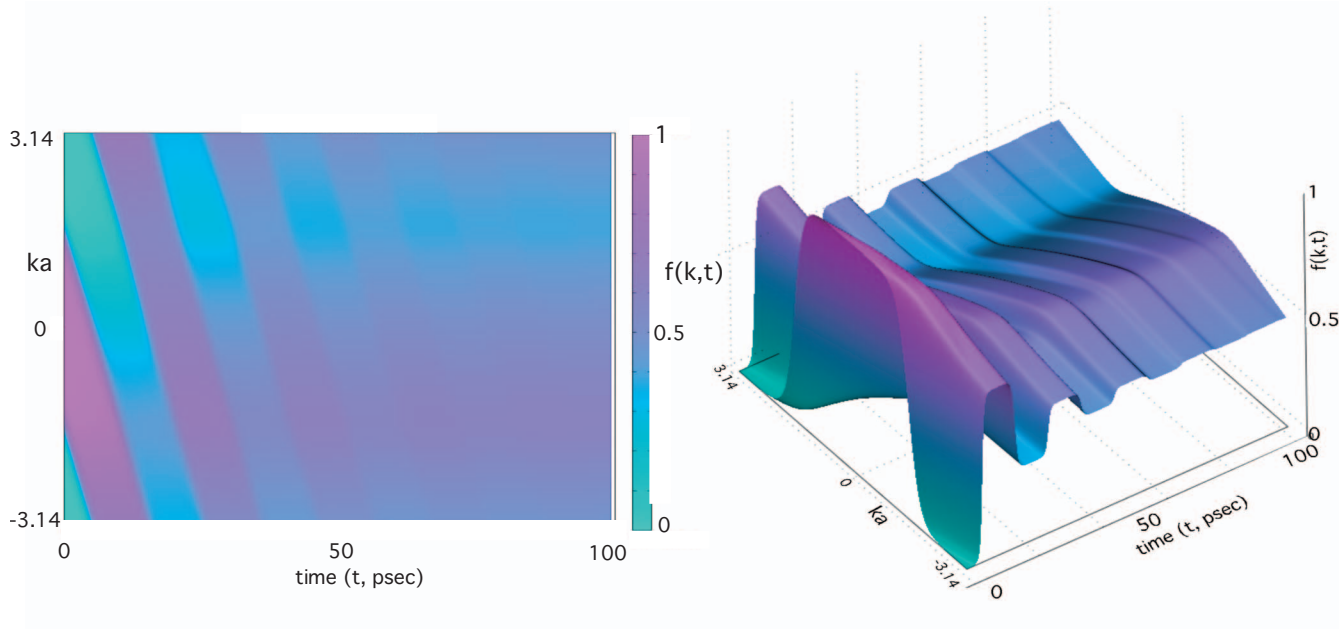

FIG. 5. (Color) (a) An image plot [i.e., the top view of (b)] and (b) a three-dimensional surface plot of the distribution function $f(k,t)$ as a function of the time (in units of picosecond) for $E=20$ V/cm, $\Delta=5$ meV, $N=10^5$ cm^{-1}, $T=4$ K, and the energy-independent scattering rates $\nu_{\rm in}=5\times10^{10}$ s^{-1} and $\nu_{\rm el}=10^{10}$ s^{-1}, relevant for the curves in Fig. 4. The function $f(k,t)$ evolves from the Fermi function $f^{(0)}(k)$ at time $t=0$ when the field is applied.

while this is not true for the two upper curves corresponding to the low field $E=5$ V/cm. The temperature dependence is contained in the Fermi factor $f_1^{(0)}$ and also implicitly in $\nu_{\rm in}$.

The properties of the steady-state current $J(\infty)$ in Fig. 1 are studied in detail in Fig. 2, which shows the current as a function of the field for several values of $(\nu_{\rm in},\nu_{\rm el})$, which are given in units of 10^{10} s^{-1}. As seen from Fig. 2 and Eq. (24), $J(\infty)$ decays as $\propto\nu_{\rm in}/E$ at high fields and becomes independent of $\nu_{\rm el}$ and linear in $\nu_{\rm in}$. The peak of the current becomes sharper for smaller $\nu_{\rm in}\nu_{\rm tr}$. Its magnitude depends only on the ratio $\nu_{\rm in}/\nu_{\rm tr}$ as predicted by Eq. (31), resulting in the same peak heights for the thin dashed–double-dotted curve for $(\nu_{\rm in},\nu_{\rm el})=(1,1)$, the thin solid curve for (5,5), and the thick solid curve for (10, 10). The position of the peaks shifts as $E\propto\sqrt{\nu_{\rm in}\nu_{\rm tr}}$. The solid curve in the upper right inset of Fig. 2 displays the temperature dependence of the prefactor $f_1^{(0)}$ for the current on the left axis. At high fields, the IV curves decay as $\propto\nu_{\rm in}f_1^{(0)}/E$ as mentioned above, where $\nu_{\rm in}$ is proportional to a factor $\lambda=1+n_{\rm ph}$. Here, $n_{\rm ph}$ is the phonon occupation number for the phonon of energy $k_BT_{\rm ph}$ and is large, viz. $n_{\rm ph}\gg1$ at high temperatures $T\gg T_{\rm ph}$. The phonon wave number along the wire for inelastic scattering can be at most $q_\parallel=2\pi/a$ and is small. The characteristic phonon energy is then on the order of $\hbar c_s q_{\rm ph}\equiv k_BT_{\rm ph}$, where $q_{\rm ph}=\sqrt{q_\parallel^2+q_\perp^2}$. Here, $q_\perp\sim1/\ell$ is the transverse component of the phonon wave vector and ℓ is the radius of the wire. The quantity $T_{\rm ph}$ is estimated to be 3.1 K for $\ell=20$ nm and $c_s\simeq5\times10^5$ cm/s. The current then depends on the temperature through the factor $Z(T)=\lambda f_1^{(0)}$, which is plotted on the right axis of the inset of Fig. 2, showing a slow temperature dependence except at low temperatures, similar to the results obtained by previous authors for three dimensions.[12,14]

For energy-dependent $\nu_{\rm el}(k)$, only the steady-state current can be readily evaluated in our model. Here, we consider the case wherein the scattering matrix element $U(q)$ is independent of the momentum transfer q relevant for a short-ranged scattering potential, yielding

$$\nu_{\rm el}(k)=\frac{\nu_{\rm el}^*}{\pi}\int_0^\pi\frac{\delta dx'}{(\cos x-\cos x')^2+\delta^2},\tag{41}$$

where $\delta=2\Gamma/\Delta\ll1$, Γ is the level damping introduced to avoid the one-dimensional van Hove singularity, and $\nu_{\rm el}^*$ is the elastic scattering rate at the center of the band (i.e., $x=ka=\pi/2$). The Fourier coefficients are then given by

$$\begin{aligned}\nu_{{\rm el},n}&\equiv\int_0^\pi\nu_{\rm el}(k)\cos(nx)dx\\&=\pi\nu_{\rm el}^*(-1)^{n/2}\int_0^\infty J_0(t)J_n(t)\exp(-\delta t)dt,\\&\quad n=\text{even},\end{aligned}\tag{42}$$

where $J_n(t)$ is the nth order Bessel function, and $\nu_{{\rm el},n}=0$ for odd integers. We calculate $J(\infty)$ from Eqs. (11), (13), (15), (22), and (23). The results are displayed in Fig. 3 for $\delta=0.01$ for the same set of values of $(\nu_{\rm in},\nu_{\rm el}^*)$ as those of $(\nu_{\rm in},\nu_{\rm el})$ studied in Fig. 2. The results are very similar not only in the shapes and magnitudes of the curves (considering the fact that $\nu_{\rm el}^*$ is somewhat different from $\nu_{\rm el}$) but also on the dependence of the peak heights and the positions on $\nu_{\rm in}$ and $\nu_{\rm el}^*$.

Figure 4 displays the evolution of the distribution function $f(k,t)$ in Eq. (32) of an electron gas driven by an electric

field of 20 V/cm for several time values corresponding to the time points (represented by the symbols) for the current versus the time curve (solid line) of Fig. 1 that is repeated in the upper inset. The system starts in equilibrium (dotted curve) at $t=0$. The distribution function is maximally shifted to the left at $t=4.7$ ps (indicated by the solid circles in Figure 4 and the inset) as shown by the thick solid curve, yielding a maximum current indicated by the solid circle in the inset. The current becomes nearly zero at $t=12$ ps (hollow square) and 19.5 ps (hollow triangle). However, the distribution functions (thin solid curve and dashed-dotted curve) are not symmetric with respect to $x=0$. The dashed–double-dotted curve represents the steady-state distribution function beyond $t>100$ ps.

Comparing the thin dotted and the thick solid curves, it is interesting to note that $f(k,t)$ is "rigidly" shifted, roughly speaking, initially to the left, yielding the maximum current at $t=4.7$ ps. During this initial short time period, scattering plays a minor role compared to the acceleration and the drift imposed by a strong field. Note that the electron distribution function already spills over to the other side, i.e., $ka\sim\pi$ at $t=4.7$, causing the current to decrease and start to oscillate. However, the maximum (minimum) value of $f(k,t)$ decreases (increases) with time, as the electrons are scattered toward the final steady state, resulting in the flatter distribution given by the dashed-double-dotted curve.

The oscillations of the distribution function and the decay of the peak amplitude toward the steady state are clearly demonstrated by an image plot of $f(k,t)$ in Fig. 5(a) and a three-dimensional surface plot in Fig. 5(b). The slanted red stripes in Fig. 5(a) and slanted ridges in Fig. 5(b) at early times indicate nearly rigid drift motion of the populated band of the electrons in k space from the initial Fermi distribution inside $-k_F\lesssim k\lesssim k_F$ toward the zone boundary at $ka=-\pi$, which are spilling over to the other zone boundary at $ka=\pi$ with increasing time. These oscillations repeat for a longer period of time for a smaller total scattering rate ν_t according to Eq. (28). Also, the oscillation frequency $\nu_{1E>}=\sqrt{\omega_E^2-\nu_{\rm el}^2}$ becomes faster for a larger field and a smaller elastic scattering rate. The red stripes in Fig. 5(a) and the ridges in Fig. 5(b) eventually decay into a uniform steady background due to diffusive scattering with time. The horizontal dark red stripe in Fig. 5(a) and the reddish ridge along the time axis in Fig. 5(b) in the region near $ka\sim-1.5$ for $t>40$ ps represent a region with a relatively larger electron population that emerges toward the steady-state. This region of enhanced electron population is also seen near $ka\sim-1.5$ from the dashed-double-dotted curve in Fig. 4.

VI. CONCLUSIONS

We have presented an exact analytic result for the time-dependent current and the evolution of the distribution function in a nonlinear electric field for a degenerate and nondegenerate electron gas in a one-dimensional superlattice miniband employing a relaxation-time approximation for inelastic scattering. Our results clearly show the distinct roles played by elastic and inelastic scattering and demonstrate the dynamics of the competition between the acceleration by the electric field and scattering by phonons and static impurities in a transparent way in producing the damped Bloch oscillations and the steady-state current. They also quantitatively show how scattering damps the Bloch oscillation, the condition for the onset of the oscillations, and also the oscillation frequency. The present approach can serve as a guide in understanding the results of a more complicated full numerical treatment. A recent full numerical study that replaces the present relaxation-time approximation of inelastic scattering by microscopic electron-phonon scattering processes yielded results very similar to those predicted here.[22]

ACKNOWLEDGMENTS

The author wishes to thank W. Pan and D. H. Huang for helpful discussions. This work was supported in part by LDRD and DOE/BES at Sandia National Laboratories. Sandia is a multiprogram laboratory operated by Sandia Corporation, a Lockheed Martin Company, for the U.S. DOE under Contract No. DE-AC04-94AL85000.

*sklyo@sandia.gov

[1] L. Esaki and R. Tsu, IBM J. Res. Dev. **14**, 61 (1970).
[2] S. A. Ktitorov, G. S. Simin, and V. Ya. Sindalovskii, Fiz. Tverd. Tela (Leningrad) **13**, 2230 (1971) [Sov. Phys. Solid State **13**, 1872 (1972)].
[3] F. G. Bass and E. A. Rubinshtein, Fiz. Tverd. Tela (Leningrad) **19**, 1379 (1977) [Sov. Phys. Solid State **19**, 800 (1977)].
[4] R. A. Suris and Shchamkhalova, Fiz. Tekh. Poluprovodn. (S.-Peterburg) **18**, 1178 (1984) [Sov. Phys. Semicond. **18**, 738 (1984)].
[5] M. Artaki and K. Hess, Superlattices Microstruct. **1**, 489 (1985).
[6] A. Sibille, J. F. Palmier, H. Wang, and F. Mollot, Phys. Rev. Lett. **64**, 52 (1990).
[7] H. T. Grahn, K. von Klitzing, K. Ploog, and G. H. Döhler, Phys. Rev. B **43**, 12094 (1991).
[8] X. L. Lei, N. J. M. Horing, and H. L. Cui, Phys. Rev. Lett. **66**, 3277 (1991).
[9] A. A. Ignatov, E. P. Dodin, and V. I. Shashkin, Mod. Phys. Lett. B **5**, 1087 (1991).
[10] R. R. Gerhardts, Phys. Rev. B **48**, 9178 (1993).
[11] A. A. Ignatov, K. F. Renk, and E. P. Dodin, Phys. Rev. Lett. **70**, 1996 (1993).
[12] S. Rott, P. Binder, N. Linder, and G. H. Döhler, Phys. Rev. B **59**, 7334 (1999).
[13] F. Löser, Yu. A. Kosevich, K. Köhler, and K. Leo, Phys. Rev. B **61**, R13373 (2000).
[14] Yu. A. Kosevich, Phys. Rev. B **63**, 205313 (2001).
[15] C. Waschke, H. G. Roskos, R. Schwedler, K. Leo, H. Kurz, and K. Köhler, Phys. Rev. Lett. **70**, 3319 (1993).
[16] R. Martini, G. Klose, H. G. Roskos, H. Kurz, H. T. Grahn, and

R. Hey, Phys. Rev. B **54**, R14325 (1996).
[17] K. Jin, M. Odnoblyudov, Y. Shimada, K. Hirakawa, and K. A. Chao, Phys. Rev. B **68**, 153315 (2003).
[18] N. Sekine and K. Hirakawa, Phys. Rev. Lett. **94**, 057408 (2005).
[19] M. Först, G. Segschneider, T. Dekorsy, H. Kurz, and K. Köhler, Phys. Rev. B **61**, R10563 (2000).
[20] V. G. Lyssenko, G. Valusis, F. Löser, T. Hasche, K. Leo, M. M. Dignam, and K. Köhler, Phys. Rev. Lett. **79**, 301 (1997).
[21] S. Rott, N. Linder, and G. H. Döhler, Phys. Rev. B **65**, 195301 (2002), and references therein.
[22] D. H. Huang (private communication).